NEOPLASIA
www.neoplasia.com

Volume 12 Number 7 July 2010 pp. 579–589 579

Microcell-Mediated Chromosome Transfer Identifies *EPB41L3* as a Functional Suppressor of Epithelial Ovarian Cancers[1,2]

Dimitra Dafou[*], Barbara Grun[*], John Sinclair[†], Kate Lawrenson[*], Elizabeth C. Benjamin[‡], Estrid Hogdall[§], Susanne Kruger-Kjaer[§], Lise Christensen[¶], Heidi M. Sowter[#], Ahmed Al-Attar[**], Richard Edmondson[††], Stephen Darby[††], Andrew Berchuck[‡‡], Peter W. Laird[§§], C. Leigh Pearce[¶¶], Susan J. Ramus[*], Ian J. Jacobs[*] and Simon A. Gayther[*]

*EGA Institute for Women's Health, Gynaecological Cancer Research Laboratories, University College London, London, UK; [†]Cancer Proteomics Laboratory, University College London, London, UK; [‡]Department of Histopathology, Royal Free/UCL Medical School, London, UK; [§]Institute of Cancer Epidemiology, Danish Cancer Society, Copenhagen, Denmark; [¶]Department of Pathology, Bispebjerg Hospital, University of Copenhagen, Copenhagen, Denmark; [#]University of Derby, Faculty of Education, Health and Science, Kedleston Road, Derby, UK; **Academic Department of Clinical Oncology, University of Nottingham, Nottingham University Hospitals, Nottingham, UK; [††]Northern Institute for Cancer Research, Newcastle Upon Tyne, UK; [‡‡]Division of Preventive Medicine, The Duke Comprehensive Cancer Center, Durham, NC, USA; [§§]University of Southern California, USC Epigenome Center, Los Angeles, CA, USA; [¶¶]University of Southern California, Department of Preventive Medicine, Keck School of Medicine, Los Angeles, CA, USA

Abstract

We used a functional complementation approach to identify tumor-suppressor genes and putative therapeutic targets for ovarian cancer. Microcell-mediated transfer of chromosome 18 in the ovarian cancer cell line TOV21G induced *in vitro* and *in vivo* neoplastic suppression. Gene expression microarray profiling in TOV21G^{+18} hybrids identified 14 candidate genes on chromosome 18 that were significantly overexpressed and therefore associated with neoplastic suppression. Further analysis of messenger RNA and protein expression for these genes in additional ovarian cancer cell lines indicated that *EPB41L3* (erythrocyte membrane protein band 4.1-like 3, alternative names DAL-1 and 4.1B) was a candidate ovarian cancer-suppressor gene. Immunoblot analysis showed that *EPB41L3* was activated in TOV21G^{+18} hybrids, expressed in normal ovarian epithelial cell lines, but was absent in 15 (78%) of 19 ovarian cancer cell lines. Using immunohistochemistry, 66% of 794 invasive ovarian tumors showed no *EPB41L3* expression

Abbreviations: MMCT, microcell-mediated chromosome transfer; *EPB41L3*, erythrocyte membrane protein band 4.1-like 3

Address all correspondence to: Simon A. Gayther, PhD, Gynaecological Cancer Research Laboratories, Paul O'Gorman Bldg, University College London, 72 Huntley St, London, WC1E 6BT, UK. E-mail: s.gayther@ucl.ac.uk

[1]This work has been funded by the Eve Appeal Gynaecology Cancer Research Fund. This work was undertaken at the University College London Hospital/University College London that received a proportion of funding from the Department of Health's National Institute for Health Research Central Biomedical Research Centers funding scheme and from the Ovarian Cancer Research Fund (grant no. PPD/USC.06).

[2]This article refers to supplementary materials, which are designated by Tables W1 and W2 and Figures W1 to W3 and are available online at www.neoplasia.com.

Received 28 February 2010; Revised 30 March 2010; Accepted 5 April 2010

DOI 10.1593/neo.10340

compared with only 24% of benign ovarian tumors and 0% of normal ovarian epithelial tissues. *EPB41L3* was extensively methylated in ovarian cancer cell lines and primary ovarian tumors compared with normal tissues ($P = .00004$), suggesting this may be the mechanism of gene inactivation in ovarian cancers. Constitutive reexpression of *EPB41L3* in a three-dimensional multicellular spheroid model of ovarian cancer caused significant growth suppression and induced apoptosis. Transmission and scanning electron microscopy demonstrated many similarities between *EPB41L3*-expressing cells and chromosome 18 donor-recipient hybrids, suggesting that *EPB41L3* is the gene responsible for neoplastic suppression after chromosome 18 transfer. Finally, an inducible model of *EPB41L3* expression in three-dimensional spheroids confirmed that reexpression of *EPB41L3* induces extensive apoptotic cell death in ovarian cancers.

Neoplasia (2010) 12, 579–589

Introduction

In 1978, Stanbridge and Wilkinson showed that the fusion between HeLa cervical carcinoma cells and normal diploid fibroblasts created somatic cell hybrids with a stable karyotype and a suppressed tumorigenic phenotype [1]. The phenotypic changes were later attributed to the effects of normal copies of human chromosomes from the normal fibroblasts, functionally complementing the genetic background of the HeLa cells [2]. These findings formed the basis of a methodological development, microcell-mediated chromosome transfer (MMCT), which enables the introduction of individual human chromosomes into cancer cells and, subsequently, the localization and identification of genes associated with a multitude of biologic mechanisms including cellular senescence, immortalization, and tumor suppression [3].

Since its development, MMCT has been used extensively as an approach to improve our understanding of tumor development. Investigators have found functional evidence for several loci scattered throughout the genome that induce neoplastic suppression in a variety of tumor types [4–8]. However, progress in taking these studies forward to the stage of identifying the genes responsible has been hampered by the limited resolution of the methodology. It has often required detailed genomic and functional mapping to reduce the chromosome of interest down to a few megabases, and this frequently proves to be a challenging and lengthy process. The advent of gene expression microarray technologies has enabled researchers to sidestep this bottleneck, and a few studies that combine MMCT analysis with gene expression profiling have now been published, leading to the identification of plausible functional candidate genes for different diseases [9–11].

Some studies have used MMCT to identify chromosomes and subchromosomal regions that cause neoplastic suppression in ovarian cancer cells [12–15]. However, these studies have yet to find definitive evidence of a role for any of the candidate genes subsequently identified in the development of ovarian cancers. Generally, the mechanisms that underlie ovarian tumor development remain poorly understood, and this continues to have a major impact on clinical intervention strategies for tackling the disease. Despite improvements in cytoreductive surgery and the initial good response of patients to platinum-based chemotherapies, there have been few improvements in the survival rates for patients diagnosed with ovarian cancer for more than three decades; approximately 65% of patients will die within 5 years of their diagnosis [16]. There are many reasons for the poor survival rates. Significantly, most patients are diagnosed with advanced stage disease; but also, there are no reliable prognostic markers for predicting clinical response and guiding treatment and no novel molecular targets expressed in ovarian tumors that have led to the development of new therapies. To identify chromosome regions that are involved in the development of ovarian cancer, we recently reported using MMCT in ovarian cancer cell lines for seven chromosomes (4, 5, 6, 13, 14, 15, and 18) that we found to be frequently deleted in primary ovarian cancers [17,18]. We found that chromosome 18 functionally suppresses the neoplastic phenotype of ovarian cancer cell lines [18]. Here we describe the identification and evaluation of 14 candidate genes located on chromosome 18 that are activated in $MMCT^{+18}$/cancer cell line hybrids. For one of these candidate genes (erythrocyte membrane protein band 4.1-like 3, *EPB41L3*), further functional evaluation in primary ovarian tumors and in three-dimensional models of ovarian cancer provided additional evidence supporting a role of *EPB41L3* in ovarian cancer development.

Materials and Methods

Microcell-Mediated Monochromosome Transfer

MMCT was performed in the TOV21G cancer cell line as previously described [18,19]. TOV21G is an epithelial ovarian cancer cell line derived from a clear cell ovarian carcinoma. Briefly, the recipient ovarian cancer cell line was fused with mouse (A9):human monochromosome donor cell lines carrying the selectable fusion gene marker hygromycin phosphotransferase. MMCT hybrids were selected from post fusion cells in medium supplemented with hygromycin B (Calbiochem, Merck Chemicals Ltd, Nottingham, UK). The *in vitro* phenotype of recipient-donor hybrids was evaluated using anchorage-dependent and -independent growth assays and invasion through a Matrigel [20]. *In vivo* tumorigenicity was assayed after intraperitoneal injection of ~2.5×10^6 cells in immunosuppressed mice as previously described [20].

Genomic Mapping of Hybrids

The chromosome 18 content of hybrids and recipient cell lines was evaluated using metaphase chromosome painting. Fluorescent whole chromosome paints (Q-Biogene, Cambridge, UK) were used to detect the transferred chromosome by *in situ* hybridization using standard protocols. A mouse pan-centromeric probe (Q-Biogene) was used to detect any mouse DNA transferred; none was present in any of the hybrids analyzed. Fifteen metaphase spreads were scored for each cell line. Microsatellite analysis of 18 markers spanning chromosome 18 (http://www.gdb.org/) was used to determine whether the transferred allele was present. Array comparative genomic hybridization analysis was performed using a

whole genome tiling-path consisting of 32,450 BAC clones (http://www.instituteforwomenshealth.ucl.ac.uk/trl/microarray_facility.html). Fluorescently labeled DNA of chromosome hybrid cell lines was hybridized against the parental cell lines. DNA samples were labeled with Cy3 or Cy5 using the Bioprime Total Labeling Kit (Invitrogen, Paisley, UK). Slides were scanned using an Axon 4000B laser scanner (Genepix, Molecular Devices, Sunnyvale, CA) at a 5-μm resolution. Raw fluorescence data were extracted using "BlueFuse" software (BlueGnome, UK) and normalized using the MANOR and LIMMA packages [21]. The $\log_2$ of fluorescence ratios (M) were plotted against genome location using BAC clone locations derived from the National Center for Biotechnology Information Human Genome build 36 (HG18).

Differential Gene Expression Analysis

Total RNA isolated from cell lines was quality control tested using a Nano assay with an Agilent Bioanalyzer 2100 (Agilent Technologies, Inc, Santa Clara, CA). RNA was converted into digoxigenin-labeled complementary RNA and hybridized to a human genome microarray system (Human Genome Survey Microarray Version 2; Applied Biosystems, Foster City, CA), which contains 32,878 probes for the interrogation of 29,098 genes. Gene expression profiles were generated in triplicate for each cell line. Data analysis was performed using Applied Biosystem's 1700 ArrayExpress software, Spotfire DecisionSite for Functional Genomics software (Goteborg, Sweden), and R version 1.9.1. Probes that were deemed undetectable were excluded from the final analyses if they had a signal-to-noise ratio less than 3. An analysis of variance was used to generate P values for statistical differences between probes. P values were adjusted for multiple comparisons as described by Benjamini and Yekutieli [22]. Genes were statistically different between groups if they had an adjusted $P < .01$ and an average fold change difference greater than 1.6. Gene ontology analysis was performed using the Panther classification system (http://www.pantherdb.org).

Real-time Polymerase Chain Reaction Analysis

Total RNA was extracted and analyzed by real-time reverse transcription–polymerase chain reaction (PCR) using optimized TaqMan Gene Expression assays (Applied Biosystems). The efficacy of 18S as an endogenous control was examined using the $2^{-\Delta Ct}$ method.

Immunoexpression Analysis

Immunoblot analysis was performed for cell lines using two primary monoclonal antibodies that recognize the *EPB41L3* protein, anti–Dal-1 monoclonal antibody from Imgenex (San Diego, CA) and anti–Dal-1 monoclonal antibody from Abcam (Cambridge, UK). Cell lysates were separated by SDS-PAGE, transferred to Immobilon P membrane (Millipore, Watford Hertfordshire, UK), probed with the primary antibody and an HRP-conjugated secondary antibody. Immunoreactive bands were visualized with the enhanced chemiluminescence system (NEN Life Sciences, Boston, MA). For immunohistochemistry analysis, tissue sections were incubated with a rabbit anti-*EPB41L3* polyclonal antibody (1:1500 dilution, kindly donated by Dr I. Newsham) using standard protocols [23]. The malignant and nonmalignant tissues were scored for *EPB41L3* by assessing the site of positive staining in the tissue. Semiquantitative scoring criteria were used for immunohistochemistry; both staining intensity and positive areas of staining were recorded. We scored *EPB41L3* positive staining calculated from the proportion of immunopositive neoplastic cells in the specimen (0, negative [<5% of positive cells]; 1, weak [5%-20%]; 2, moderate [20%-50%]; 3, strong [>50%]).

DNA Methylation Analysis

Cell line analyses. Quantitative DNA methylation analysis was performed in ovarian cancer and normal ovarian epithelial cell lines using the MassARRAY EpiTYPER (Sequenom, San Diego, CA) after DNA bisulfite treatment and matrix-assisted laser desorption ionization time-of-flight mass spectrometry analysis. Mass spectra were acquired by using a MassARRAY Compact MALDI-TOF, and the spectra's methylation ratios were generated by the Epityper software v1.0 (Sequenom). The *EPB41L3* promoter was analyzed in three PCR amplicons, designed using EpiDesigner software (Sequenom). In total, 154 CpG sites in *EPB41L3* were analyzed.

Primary tissue analyses. A total of 45 invasive ovarian cancer tumor tissue samples (of various histologic subtypes) and 16 normal tissue samples (endometrial, peritoneal, and fallopian tube tissues) were analyzed for 20,000 probes using the Illumina Infinium (Illumina, San Diego, CA) "genome-wide" panel after extraction and bisulfite conversion of DNA. Tissue samples were collected from Duke University and the University of Southern California; the analysis had ethical committee approval. All data were analyzed using Genetrix/SB version 3.3 (Epicenter Software, Alhambra, CA). The mean methylation values between the tumor and normal samples for each of these probes were compared using a parametric t test.

Expressing EPB41L3 in Ovarian Cancer Cell Lines

For continuous expression, *EPB41L3* complementary DNA (cDNA) was cloned into a pBMN expression vector and transfected into three epithelial ovarian cancer cell lines: TOV21G, SCOV3, and INTOV2 using FuGENE 6 Transfection Reagent (Roche, Welwyn, UK). Briefly, 10^6 cells were transfected with the gene expression vector or a control vector expressing the GFP reporter gene (Orbigen, San Diego, CA). Selection was performed using 500 μg/ml geneticin (Sigma-Aldrich, St Louis, MO), and cells expressing the plasmids were subcultured by ring cloning. Stably transfected cell lines expressing *EPB41L3* were established as multicellular spheroids by culturing cells in 1% agarose-coated 24 multiwell plates. Spheroids were visualized using an inverted microscope to calculate spheroid size and volume. The projected area, A and perimeter P, for each spheroid were measured using IMAGE J software (http://rsbweb.nih.gov/ij/). Spherical volume and geometric mean diameter of each spheroid were calculated as previously described [24].

Conditional EPB41L3 Expression

The Ecdysone muristerone–induced system (gift from Irene Newsham) was used to generate an inducible TOV21G-*EPB41L3* expressing cell line. Transfection of the retinoid-X receptor containing vector (pVgRXR) was followed by the pIND- *EPB41L3* vector, and the doubly transfected clones were selected with 35 μg/ml zeocin (Invitrogen) and 600 μg/ml geneticin (Sigma). Approximately 30 clones were screened by *EPB41L3* specific fluorescence activated cell sorting (FACS) analysis for controlled inducible expression after 48 hours of 1 μM muristerone (Invitrogen) exposure. The clones generated from the inducible expression of EPB41L3 in ovarian cancer cells were screened for EPB41L3 protein expression by FACS analysis to identify a clone expressing high levels of EPB41L3 (>65% of cells expressed the protein) for use in downstream experiments. Multicellular spheroids were formed by culturing cells in poly-HEMA (Sigma)–coated vessels as previously described [25,26].

Assaying Apoptosis and Live/Dead Proportionality in Spheroids

Apoptosis was measured using the Annexin-V–FLUOS staining kit (Roche) according to the manufacturers instructions. Briefly, 10^6 cells were washed with PBS and were stained with annexin V and propidium iodide for 15 minutes at room temperature and analyzed using a flow cytometer (Becton and Dickinson, Oxford, UK). Live/dead assays were performed after induction of *EPB41L3* expression using a commercially available live/dead viability and cytotoxicity assay (Molecular Probes, Invitrogen). Spheroids were stained with 2 mM calcein and 4 mM ethidium homodimer 1 for 30 minutes at room temperature, and image capture was performed using a confocal microscope (Ultraview; Perkin Elmer, Cambridge, UK).

Transmission and Scanning Electron Microscopy

Spheroids were washed with phosphate-buffered saline and fixed with 2% paraformaldehyde, 1.5% glutaraldehyde in 0.1 M cacodylate buffer, pH 7.3, then washed in 0.1 M cacodylate buffer and postfixed with 1% osmium tetroxide in 0.1 M cacodylate buffer. Finally, spheroids were washed in 0.1 M cacodylate buffer before being stained with 0.5% uranyl acetate and dehydrated with ethanol. For transmission electron microscopy (TEM), spheroids were embedded in agar resin, sectioned, and examined on a JEOL 1010 TEM microscope (Jeol Ltd, Tokyo, Japan). For scanning electron microscopy (SEM), samples were postfixed with 1% osmium tetroxide in 0.1 M cacodylate buffer pH 7.3 before dehydrating with ethanol, critical point drying, mounting on carbon stubs, and coating with gold before viewing under a JEOL 7401 series FEGSEM (Jeol Ltd).

Results

Identifying Candidate Tumor-Suppressor Genes on Chromosome 18

We have previously shown that chromosome 18 induces neoplastic suppression of the epithelial ovarian cancer cell line TOV21G both *in vitro* and *in vivo* (Table W1) [18,27]. To identify candidate tumor-suppressor genes located on chromosome 18, we used gene expression microarrays to compare 29,098 different genes between the ovarian cancer cell TOV21G and two TOV21G^{+18} hybrids. The aim was to identify genes that showed an increase in expression in TOV21G^{+18} hybrids, which may suggest that they are functionally activated and responsible for the suppression phenotype. We found 14 chromosome 18 genes that were significantly overexpressed in both TOV21G^{+18} hybrids compared with the TOV21G cell line (Table 1). The locations of these genes with respect to mapping data for chromosome 18 in the hybrids are illustrated in Figure 1*A*. Semiquantitative RT-PCR analysis of 10 of these genes was used to validate the results of gene expression microarray analysis and showed the same trend in expression change for all 10 genes compared with the microarray expression data (data not shown).

For the 14 candidate genes, we reviewed the evidence of a role in cancer based on their known or putative function and any experimental data from previously published studies. On the basis of this analysis, we restricted the list of plausible candidates to 11 genes, which we evaluated further by analyzing gene and protein expression (if antibodies were available) in a panel of 19 ovarian cancer cell lines and 3 normal ovarian epithelial cell lines (Table 1). These analyses suggested that one candidate gene in particular, *EPB41L3* (the erythrocyte membrane protein band 4.1-like 3 gene or alternative nomenclature DAL-1), at 18p11.32 is a candidate ovarian cancer-suppressor gene.

Evaluating EPB41L3 as an Ovarian Cancer-Suppressor Gene

Expression microarray analysis indicated that *EPB41L3* was more than 50-fold overexpressed in TOV21G^{+18} hybrids compared with its expression in TOV21G cells (Figure 1*B*). Microsatellelite analysis confirmed that this gene had been transferred into both TOV21G hybrids (data not shown). The high level of increased expression in the TOV21G^{+18} hybrids suggested that the gene had been activated as result of the chromosome transfer. Consistent with this, most genes flanking *EPB41L3* showed only minor variation in the levels of differential gene expression between TOV21G and TOV21G^{+18} cells (Figure 1*A*).

Table 1. Candidate Ovarian Cancer Tumor Suppressor Genes Identified by Differential Gene Expression Analysis of the TOV21G Cell Line and the MMCT Hybrids TOV21G$^{+18.1}$ and TOV21G$^{+18.2}$.

Gene	Differential Microarray Expression Analysis		Cancer Cell Line Expression		Putative Function*	References†
	FC‡	*P*§	RNA¶	Protein#		
EMILLIN 2	11.67	3.00e–03	36%	15%	Extracellular matrix glycoprotein cell adhesion overexpressed in ovarian tumors	[15]
KNTC2	0.03	8.11e–05	21%	10%	Mitotic spindle check protein overexpressed in tumors	[4]
EPB41L3	50.2	8.11e–06	89%	79%	Tumor suppressor: underexpressed in lung, breast, and prostate cancers	[7,8,9]
RALBP1	2.43	.001	ND	NA	Membrane traffic protein; overexpressed in ovarian, lung cancer	[2]
CDH2	16.6	.003	52%	70%	Cadherin, cell adhesion-wnt signaling pathway; overexpressed in epithelial tumors	[12]
SNRPD1	3.5	.0003	ND	NA	Small nuclear riboprotein-promotes snRNP assembly, messenger RNA splicing factor	[6]
KIAA1632	8.6	.0002	ND	NA	Molecular function unclassified	NR
CCDC5	1.9	.009	52%	0%	Regulation of spindle function, cell cycle control	[5]
MYO5B	6.3	.001	21%	NA	actin binding motor protein, methylated in leukemias	[11]
TCF4	145	6.36e–06	10%	0%	Transcription factor, cell proliferation-differentiation	[10]
ZNF532	0.1	3.92e–06	52%	NA	KRAB box transcription factor	SR [14]
C18ORF22	3	4.36e–06	ND	NA	Molecular function unclassified	NR
SDCCAG33	2.9	4.97e–07	57%	NA	Zinc finger transcription factor, colon cancer antigen	[3,14]
CYB5	2.1	.004	ND	NA	Steroid metabolism	[3]

NA indicates antibody not available; *ND*, RT-PCR not done.

*Putative gene function and role in carcinogenesis: information obtained from Panther Ontology and Genecards databases.

†References used to evaluate the significance of each candidate gene are provided in Supplementary Information 1. *NR* indicates no reference; *SR*, supplementary reference number.

‡Average fold change overexpression in two MMCT hybrids compared with the parental ovarian cancer cell line.

§Statistically significant difference in expression between two MMCT hybrids and the parental ovarian cancer cell line.

¶Semiquantitative RT-PCR analysis comparing the average gene expression of three normal ovarian epithelial cell lines (normalized to the endogenous control gene *18S*) and gene expression in each of 19 different epithelial ovarian cancer cell lines. The figure given for each gene represents the proportion of ovarian cancer cell lines that show reduced expression compared with normal cell expression.

#The proportion of ovarian cancer cell lines that showed complete absence of protein expression (measured by immunoblot analysis) for genes where antibodies were available.

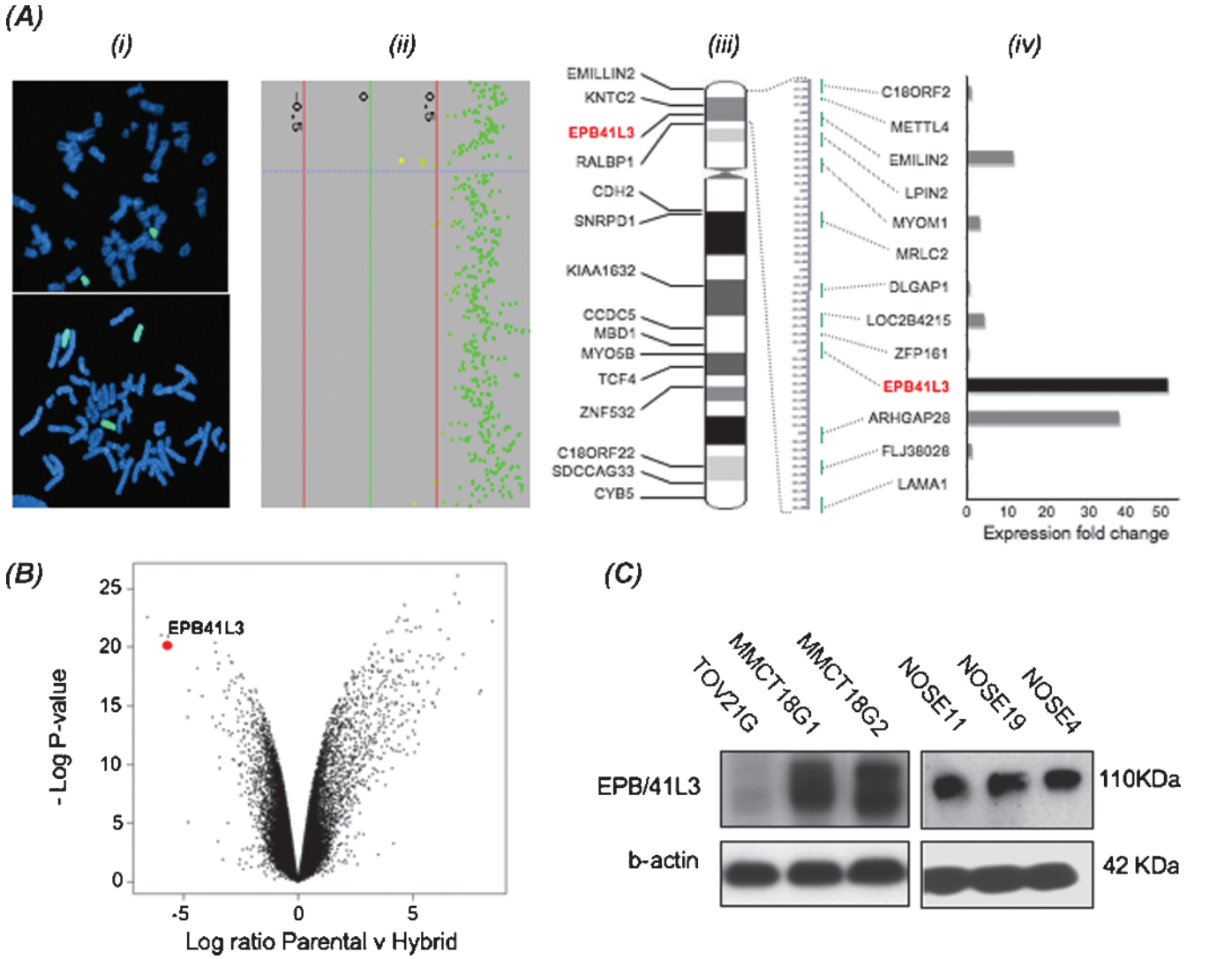

Figure 1. (A) Genomic mapping and candidate gene identification in TOV21G^{+18} hybrids confirm the transfer of chromosome 18 material in parental cancer cell lines. (i) Metaphase fluorescence *in situ* hybridization (FISH) using a chromosome 18 paint of TOV21G cells (top panel) and TOV21G^{+18} cells (bottom panel) confirms the transfer of a single additional copy of chromosome 18 (green fluorescent staining) in the hybrid cells. (ii) Microarray CGH analysis confirms the results of FISH and provide more detailed mapping information of TOV21G^{+18} cells. Microarray CGH profiles show copy number difference between parental and hybrid cell line for a tiling path of bacterial artificial chromosomes (BACs) spanning the length of chromosome 18. Green spots indicate single copy number gain. Mapping showed the same regions transferred for both hybrids used in expression analysis of each cell line. (iii) The location of genes on chromosome 18 identified by differential gene expression microarray analysis of the TOV21G cancer cell line compared with two MMCT hybrids. The candidate gene *EPB41L3*, which was taken forward for further analyzes, is highlighted in red. (iv) The expression fold change for the *EPB41L3* gene and flanking genes in TOV21G cells suggest the activation of *EPB41L3*. (B) Volcano plot showing the gene expression data from chromosome 18 in TOV21G^{+18} hybrids compared with TOV21G cancer cells. The color point showing the magnitude of fold change in EPB41L3 gene expression (*x*-axis), coupled with statistical significance (*y*-axis: $-\log_{10}$ of the *P* value). (C) Immunoblot analysis using a EPB41L3 monoclonal antibody suggests a lack of expression in TOV21G cells but strong expression in both TOV21G^{+18} hybrids (MMCT18G1 and MMCT18G2), suggesting that EPB41L3 is activated in hybrid cells. EPB41L3 is also highly expressed in two primary normal ovarian surface epithelial cell cultures (NOSE11 and NOSE19) and in an immortal ovarian surface epithelial cell line (IOSE4); 110 kDa is the expected and observed size of the EPB41L3 protein band.

Immunoblot analysis confirmed the absence of EPB41L3 protein in TOV21G cells and a strong expression in both of the TOV21G^{+18} hybrid cell lines (Figure 1*C*). Three normal ovarian surface epithelial cell lines also showed high levels of EPB41L3 expression.

EPB41L3 protein expression was further evaluated in ovarian cancer cell lines and tissues from primary invasive epithelial ovarian cancers, benign epithelial ovarian tumors, and normal ovarian epithelium by Western blot analysis and immunohistochemistry. EPB41L3 expression was absent in 15/19 ovarian cancer cell lines (79%; Figure 2*A*). Immunohistochemical staining of 794 invasive and 33 benign tumors distributed across tissue arrays from three different studies showed no identifiable EPB41L3 expression in 65% of all invasive tumors and minimal, partial or complete expression in 20%, 10%, and 5% of these tumors, respectively (*P* trend = .01). When tumors were stratified by histologic subtype, clear cell, serous, mucinous, and endometrioid subtypes showed the most frequent loss of EPB41L3 expression (69%, 66%, 61%, and

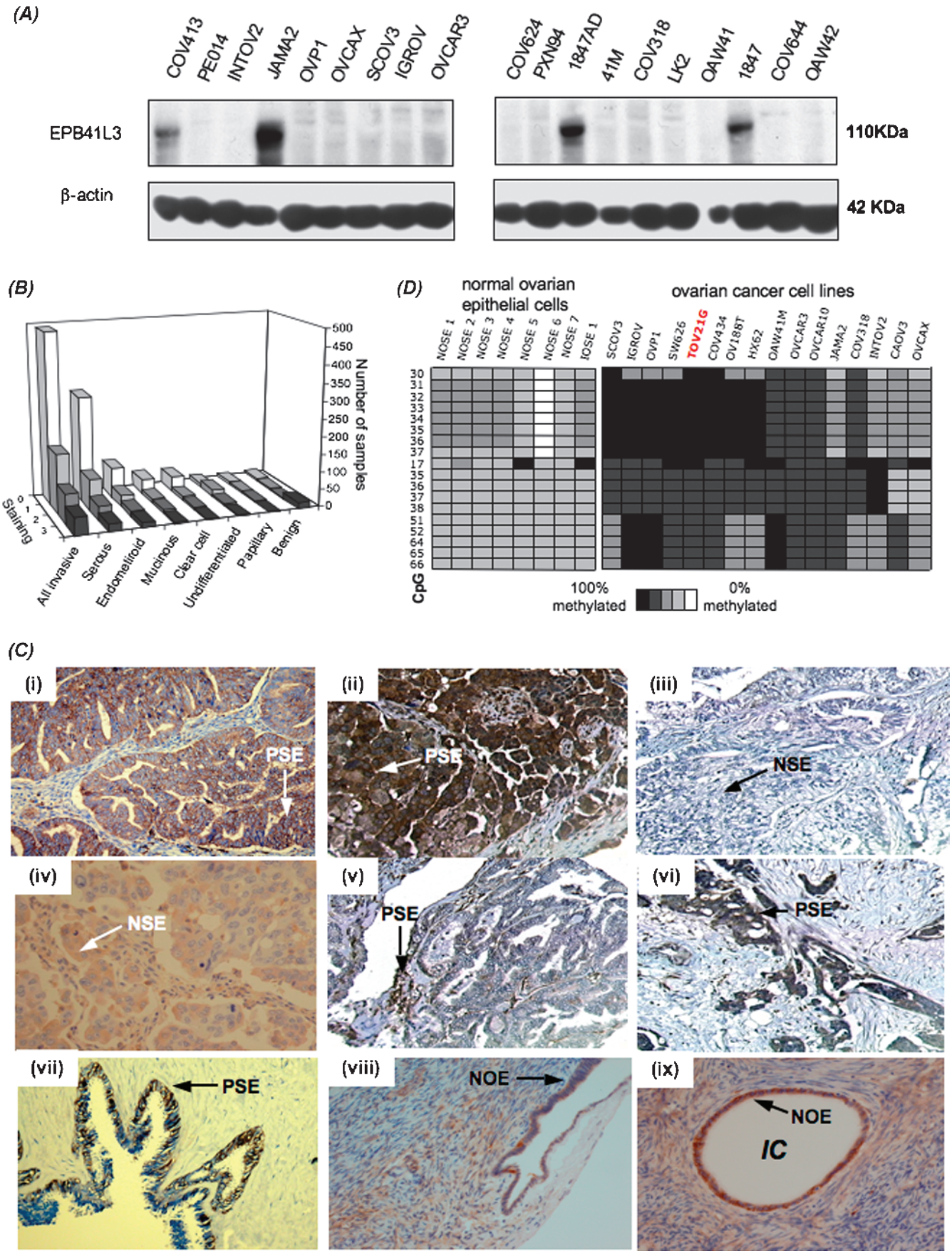
(A)
COV413
PE014
INTOV2
JAMA2
OVP1
OVCAX
SCOV3
IGROV
OVCAR3
COV624
PXN94
1847AD
41M
COV318
LK2
OAW41
1847
COV644
OAW42
EPB41L3
110KDa
β-actin
42 KDa
(B)
Number of samples
Staining
All invasive
Serous
Endometrioid
Mucinous
Clear cell
Undifferentiated
Papillary
Benign
(D)
normal ovarian epithelial cells
ovarian cancer cell lines
NOSE 1
NOSE 2
NOSE 3
NOSE 4
NOSE 5
NOSE 6
NOSE 7
IOSE 1
SCOV3
IGROV
OVP1
SW626
TOV21G
COV434
OV188T
HX62
OAW41M
OVCAR3
OVCAR10
JAMA2
COV318
INTOV2
CAOV3
OVCAX
CpG
100% methylated
0% methylated
(C)
(i)
PSE
(ii)
PSE
(iii)
NSE
(iv)
NSE
(v)
PSE
(vi)
PSE
(vii)
PSE
(viii)
NOE
(ix)
NOE
IC

57%, respectively). In contrast, there was no evidence of loss of EPB41L3 expression in 55% of benign tumors and in all five normal ovarian epithelial tissue samples. These data are illustrated in Figure 2, *B* and *C* (see also Table W2).

Studies in other cancers suggest that methylation of the *EPB41L3* promoter is a common mechanism by which the gene is downregulated during tumor development. Therefore, we examined the methylation status of *EPB41L3* in 16 ovarian cancer cell lines and 8 normal ovarian epithelial cell lines using a semiquantitative approach that enabled us to examine the methylation status at all CpG sites for the gene (Supplementary Information 2). Most ovarian cancer cell lines, including TOV21G, showed extensive methylation at the *EPB41L3* locus, whereas normal ovarian epithelial cells showed hypomethylation relative to cancer cells (Figure 2*D*). We also analyzed the methylation status of *EPB41L3* and other genes in the flanking regions in 45 primary invasive ovarian tumors and 16 normal primary tissue samples (endometrium, peritoneum, and fallopian tube). This was part of a genome-wide methylation analysis of approximately 20,000 probes (data not shown). Of the 32 probes from the 7.9-Mb region surrounding *EPB41L3*, which contains 22 genes, only 2 probes showed a statistically significant difference in the mean methylation values between tumor and normal samples: *RALBP1* (P = .016) and *EPB41L3* (P = .00004). When all probes located on chromosome 18 (n = 304) were analyzed and a false discovery rate of 0.05 was applied (equivalent to P = .003), *EPB41L3* was one of only 19 probes that showed a statistically significant difference in mean methylation values.

Functional Effects of Reexpressing EPB41L3 in Ovarian Cancer Cells

A full-length normal *EPB41L3* cDNA, cloned into a pBMN expression vector, was transfected into three ovarian cancer cell lines: TOV21G (TOV21G$^{+EPB41L3}$), SCOV3 (SCOV3$^{+EPB41L3}$), and INTOV2 (INTOV2$^{+EPB41L3}$). After confirming the reexpression of *EPB41L3* in TOV21G, we evaluated the effects on anchorage-dependent and -independent growth and compared these phenotypes with those of the same cells transfected with an empty pBMN vector expressing GFP (TOV21G^{+GFP}, SCOV3^{+GFP}, and INTOV2^{+GFP}). *EPB41L3*-expressing cells formed significantly fewer colonies than GFP-transfected cells and untransfected cells. The colonies that did form after *EPB41L3* transfection were substantially more disparate and showed markedly decreased anchorage-dependent and -independent growth (Supplementary Information 3).

We established three-dimensional multicellular spheroids of TOV21G, INTOV2, and SCOV3 ovarian cancer cell lines, of the GFP- and *EPB41L3*-expressing forms of these cell lines and of TOV21G^{+18} hybrids (Supplementary Information 3). Macroscopically and microscopically, the spheroids that formed from TOV21G, INTOV2, and SCOV3 cell lines and from GFP-expressing cells shared similar phenotypic characteristics, with no significant differences in their size. In contrast, spheroids formed from TOV21G^{+18} hybrids and *EPB41L3*-transfected cancer cell lines were significantly smaller compared with parental cell lines, consistent with the postulated tumor-suppressive effects of *EPB41L3* (P > .0001 for size and P > .0001 for volume; Figure 3, *A* and *B*). The structural and morphologic features of parental cell lines also changed substantially after *EPB41L3* transfection, shown by SEM and TEM (Figure 3*C*). For example, TOV21G cells revealed structures consistent with their epithelial origin (secretion of an extracellular matrix; tight junctions, desmosomes, and microvilli; lumens forming within spheroids). However, spheroids established from TOV21G^{+18} and TOV21G$^{+EPB41L3}$ cells showed less cell aggregation and membrane interactions (smooth contours), clear signs of increased apoptosis in surface cells, large cell surface protrusions (including filopodia and microspikes), and degenerating cell membranes. FACS analysis for annexin V confirmed that the transfer of chromosome 18 or reexpression of *EPB41L3* in TOV21G, INTOV2, and SCOV3 cells induces apoptosis (Figure 3*D*).

Finally, we evaluated the effects of inducing *EPB41L3* expression after the formation of spheroids using an Ecdysone muristerone–inducible system. We generated an inducible TOV21G$^{+EPB41L3/ECD}$ cell line and used FACS analysis to confirm *EPB41L3* expression after muristerone induction (data not shown). A fluorescent live/dead assay was used to evaluate apoptosis in spheroids. Ten days after *EPB41L3* induction, the ratio of "live" to "dead" (apoptotic) spheroids was significantly lower than it was for the same cells without *EPB41L3* induction (1:3 *vs* 6:1, P < .002; Figure 3*E*).

Discussion

Using a functional complementation approach, we have identified *EPB41L3* as a candidate tumor-suppressor gene for ovarian cancer. The gene is extensively methylated in ovarian cancer cell lines and primary

Figure 2. Evaluating *EPB41L3* status in primary ovarian cancers, ovarian cancer cell lines, and normal ovarian epithelial cell lines and tissues by immunohistochemistry and methylation analyses. (A) Immunoblot analysis for EPB41L3 in ovarian cancer cell lines shows absence of expression in 15 (79%) of 19 cell lines. (B) Illustration of EPB41L3 expression analyzed in 794 invasive ovarian cancer specimens (stratified by histologic subtype) and 33 benign ovarian tumors. Staining values: 0, less than 5% of neoplastic cells stain positive; 1, 5% to 20%; 2, 20% to 50%; 3, more than 50%. Immunohistochemistry was performed for invasive ovarian cancers and benign tumors established as tissue arrays taken from three ovarian tumor tissue collections: the Danish MALOVA study (488 ovarian tumors) [23], the Derby City Hospital tumor array (263 ovarian tumors), and the Newcastle ovarian cancer tissue micro array (160 invasive tumors) [41]. Normal primary epithelial tissues and additional invasive ovarian tumors were provided by the University College London Hospital ovarian tumor tissue biobank. (C) Examples of immunohistochemical staining with EPB41L3. Where we observed EPB41L3 staining, it suggested that EPB41L3 protein expression occurs uniformly throughout the cytoplasm and in cell membranes of both tumor and normal cells. All panels are 200× magnification: (i) 100% expression in an endometrioid ovarian cancer, (ii) 90% expression in a serous ovarian cancer, (iii) 0% expression in an endometrioid ovarian cancer, (iv) 50% expression in an endometrioid ovarian tumor, (v) 10% expression in a serous ovarian tumor (vi), 20% expression in a serous ovarian cancer, (vii) 30% expression in an endometrioid ovarian cancer, (viii) 100% expression in normal ovarian surface epithelial cells, and (ix) 100% expression in normal ovarian epithelial cells in an inclusion cyst. *IC* indicates inclusion cyst; *NOE*, normal ovarian epithelium; *NSE*, negative staining epithelium; *PSE*, positive staining epithelium. (D) Heat map illustrating methylation analysis of the *EPB41L3* promoter in normal ovarian surface epithelial cell lines and 16 ovarian cancer cell lines. Each feature represents the methylation status at a CpG dinucleotide in the promoter region. The darker the feature, the more hypermethylated the CpG. Combining the data, for all CpGs, 74% of CpGs showed greater than 60% methylation in ovarian cancer cell lines; only 1% of CpGs were more than 60% methylated in the normal ovarian epithelial cell lines.

tumor tissues compared with normal epithelial ovarian cells and primary normal tissues, EPB41L3 protein expression is completely lost in 65% of all primary invasive ovarian tumors and in 79% of ovarian cancer cells lines, and reexpression of the gene in three-dimensional ovarian cancer cell line models causes growth suppression and increased apoptosis. To our knowledge, this is the first report linking *EPB41L3* to ovarian carcinogenesis.

In the past, MMCT has been successful at identifying chromosome and subchromosomal regions that are associated with a disease phenotype or functional mechanism but rarely has definitive evidence for a specific

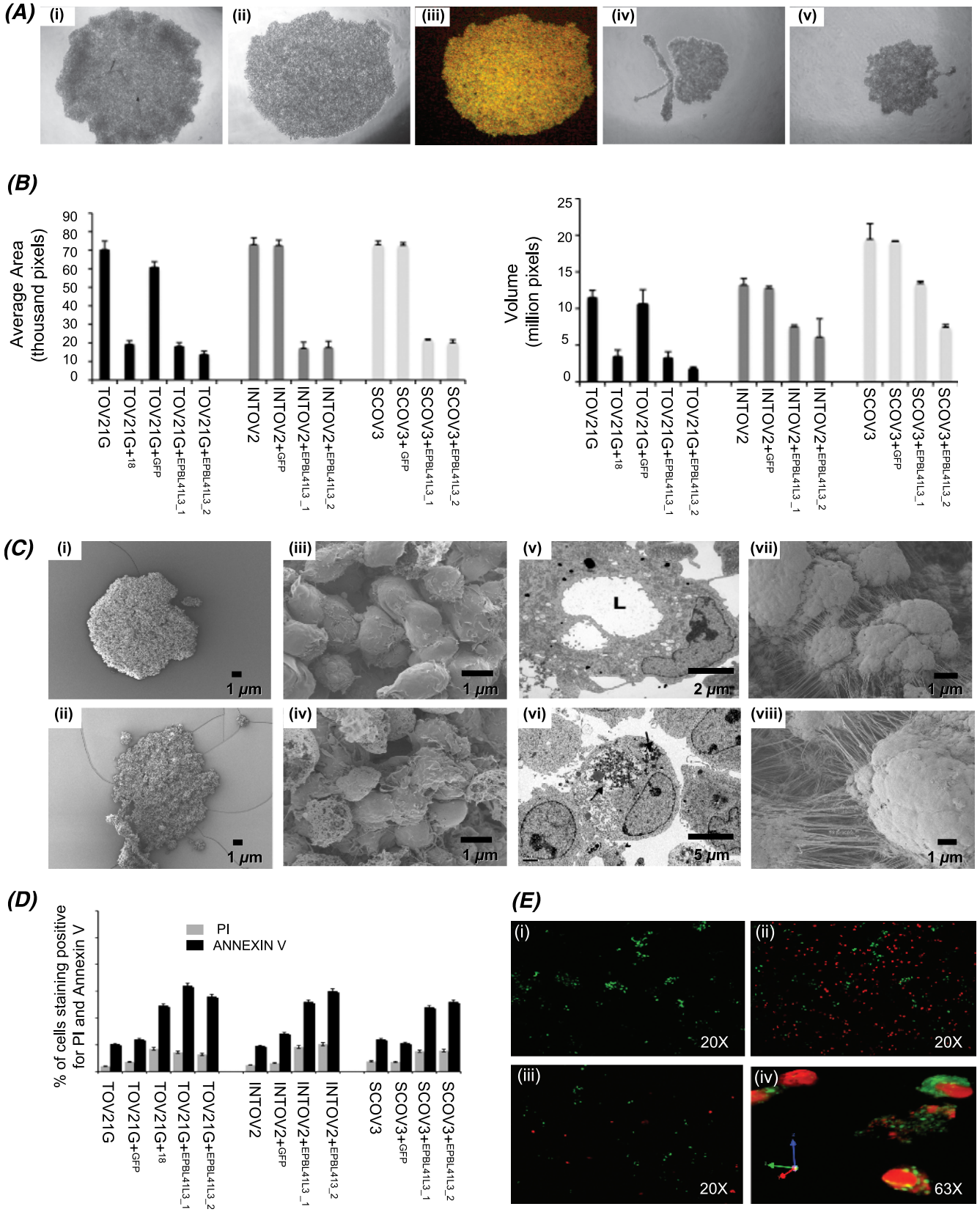

gene responsible for the observed phenotype been shown. Largely, this is because of the scale of the task in fine mapping the chromosome region of interest and then evaluating several putative candidate genes. The task is made greater still because there are several mechanisms by which the function of a gene can be abrogated (e.g., coding sequence mutation, promotor methylation, gene deletion), and evaluating each possible mechanism is a major challenge. In the current study, the approach we used identified a relatively small series of candidate genes that were associated with neoplastic suppression, caused by chromosome 18 transfer into an ovarian cancer cell line. Additional analysis based on known function and the molecular analysis of several ovarian cancer cell lines suggested that *EPB41L3* was the strongest candidate; but it remains a possibility that one or more of the other identified genes, or an as yet unidentified gene, is the real cause of neoplastic suppression. Following up on one or several of the other candidate genes we identified will require additional and extensive functional analyses to establish if they have a role in ovarian carcinogenesis.

Some studies have successfully identified the gene responsible for the phenotype after MMCT, which shows the power of this methodological approach. For example, two recent MMCT studies have found two genes, *cblD* on chromosome 2q23.2 and *cblF* on chromosome 6q13 that are involved in vitamin B_{12} metabolism [28,29]. In our study, the evidence that *EPB41L3* is the chromosome 18 gene that causes neoplastic suppression in TOV21G is compelling. The phenotypic features of *EPB41L3*-expressing cells and TOV21G^{+18} hybrids are remarkably similar in the macroscopic and microscopic appearance of multicellular spheroids and in their growth characteristics and apoptotic phenotype. The analysis of *EPB41L3* in cancer cell lines and primary tumors provides strong evidence that *EPB41L3* is an ovarian cancer-suppressor gene. Immunohistochemistry analysis of more than 800 ovarian tumors found that *EPB41L3* is downregulated in approximately two-thirds of all major histologic subtypes of ovarian cancer but is strongly expressed in normal ovarian epithelium. It is uncommon to find a molecular marker that shows a similar pattern of expression in all the major ovarian cancer subtypes. A recent study by Kobel et al. [30] analyzed 21 candidate tissue biomarkers in 500 invasive ovarian tumors and found extensive variation in the patterns of expression between high-grade serous, clear cell, endometrioid, and mucinous ovarian carcinomas for almost all markers tested. However, immunohistochemistry alone does not provide sufficient evidence that a gene is essentially involved in tumor development. It is possible that *EPB41L3* is merely a marker for a functionally relevant biologic mechanism or pathway involved in ovarian cancer progression. Therefore, it was important to identify the mechanism by which EPB41L3 was downregulated. Previous studies have shown that *EPB41L3* is hypermethylated in non–small cell lung cancers, hepatocellular carcinomas, meningiomas, renal clear cell carcinomas, and prostate carcinomas [31–34]. Another study suggests that functionally significant somatic mutations of *EPB41L3* are probably rare [35]. We tested and found evidence for extensive *EPB41L3* promoter hypermethylation in ovarian cancer cell lines and primary ovarian tumors compared with normal cells, suggesting that this is the likely cause of EPB41L3 down-regulation in ovarian tumors.

EPB41L3 expression was more prominent in benign ovarian tumors, and all normal ovarian epithelial cells analyzed showed strong expression. This possibly indicates that loss of EPB41L3 expression is a late rather than an initiating event in ovarian cancer progression. This is supported by *in vivo* data, which show that mice deficient for *EPB41L3* develop normally and are fertile. Rates of cellular proliferation and apoptosis in brain, mammary, and lung tissues from the *EPB41L3* null mice were similar to those in wild-type mice, and there was no evidence that null mice were susceptible to tumor development [36]. However, when *EPB41L3*-null mice are crossed with TRAMP mice, which express SV40 in the prostate, mice have a much greater propensity to develop aggressive, spontaneous prostate carcinomas compared with TRAMP mice alone [37]. The known functions of *EPB41L3* are also consistent with a role for the gene in the later stages of tumor development. *EPB41L3* is a member of the band 4.1 family of cytoskeletal proteins, which includes ezrin, radixin, moesin, and merlin. These proteins participate in organizing the actin cytoskeleton and ensure stable cell-cell adhesion. It is well known that interrupting the mechanisms that regulate cell adhesion leads to increased growth, invasion, and metastasis in tumor cells; these features are characteristic of the phenotypic changes we observed in the current study after transferring chromosome 18 and, subsequently, *EPB41L3* into ovarian cancer cells. Two other studies have shown that reexpressing *EPB41L3* in the MCF7 breast cancer cell line both increases cell adhesion and induces apoptosis [38,39].

We used an *in vitro* three-dimensional modeling approach to test the functional effects of reexpressing *EPB41L3* in ovarian cancer cell lines

Figure 3. Functional effects of reexpressing *EPB41L3* cDNA in the TOV21G ovarian cancer cell line. (A) Spheroid formation in (i) TOV21G cells, (ii) TOV21G^{+GFP} cells, (iii) TOV21G^{+GFP} cells under fluorescent microscopy showing expression of green fluorescent protein, (iv) TOV21G^{+18} hybrid, and (v) TOV21G$^{+EPB41L3}$ cells. (B) Analysis of average spheroid volume and area for six replicates in two independent experiments in the ovarian cancer cell lines TOV21G, INTOV2, and SCOV3; their respective GFP-transfected lines TOV21G^{+GFP}, INTOV2^{+GFP}, and SCOV3^{+GFP}; EPB41L3-expressing spheroids TOV21G$^{+EPB41L3}$, INTOV2$^{+EPB41L3}$, and SCOV3$^{+EPB41L3}$; and the chromosome 18–transferred spheroids, TOV21G^{+18}. EPB41L3-expressing and chromosome 18–transferred spheroids show significantly reduced size and volume compared with parent and GFP-expressing cancer cell lines. (C) SEM/TEM analysis of TOV21G spheroids: (i) TEM analysis of TOV21G spheroids shows a well-defined compact structure. (ii) TEM analysis of TOV21G$^{+EPB41L3}$ spheroids shows a more diffuse structure. (iii) At higher magnification, TOV21G spheroids display a smooth outer surface, indicative of good cellular interactions and secretion of extracellular matrix. (iv) In contrast, TOV21G$^{+EPB41L3}$ spheroids show degenerating cell membranes, characteristic of apoptosis. (v) Electron micrographs of sections of TOV21G spheroids show polarized cells and the formation of lumens (L) (a characteristic of epithelial cells). (vi) Micrographs TOV21G$^{+EPB41L3}$ sections show chromatin condensation, large numbers of phagocytosomes, and vacuoles (black arrows), which are characteristics of apoptotic cells. (vii, viii) Striking similarities between TOV21G^{+18} and TOV21G$^{+EPB41L3}$ spheroids, which include large cell surface protrusions (filopodia and microspikes). (D) FACS analysis for simultaneous staining of annexin V (apoptotic cells) and propidium iodide (necrotic cells) show increased levels of apoptosis in TOV21G^{+18} hybrids and EPB41L3-expressing cells compared with untransfected TOV21G, INTOV2, and SCOV3 cell lines and their respective GFP-expressing cells. (E) Inducing *EPB41L3* expression in TOV21G spheroids. Fluorescent live-dead viability assays compare the proportion of live (viable) spheroids (green fluorescence) and dead (apoptotic) spheroids (red fluorescence). (i) Two days after induction of *EPB41L3*, more than 90% of spheroids are viable (ratio of live to dead spheroids is 15:1). (ii) Ten days after induction, more than 70% of the spheroids had undergone apoptosis (live-dead ratio 1:3). (iii) Some apoptosis was also seen in noninduced spheroids after 10 days (<20%; live-dead ratio 6:1). (v) Higher magnification shows live-dead spheroids 10 days after induction of *EPB41L3* expression.

because we have previously shown that three-dimensional culture models are much more reflective of the *in vivo* phenotype than traditional two-dimensional monolayer cultures [25,26]. To our knowledge, this is the first time that such an approach has been used to study the functional effects of expressing individual genes in cancer cells. The data provide support for the suppressive effects of *EPB41L3* reexpression in ovarian cancer cells and show that this expression induces apoptosis and restricts cell adhesion; spheroids generated from three *EPB41L3*-expressing ovarian cancer cell lines were visibly less compact than spheroids formed from the cancer cells without *EPB41L3*. These studies also suggest that this three-dimensional system could be suitable for evaluating novel therapeutic targets for ovarian cancer and that *EPB41L3* may be one such target. An alternative (or combinational) therapeutic approach to the current broad-based regimens of platinum chemotherapies (carboplatin and paclitaxal) might be to use gene replacement therapy coupling tissue- and tumor-specific gene delivery to provide high levels of gene expression– and tumor-targeted cell death. Recent studies have used constructs that tightly control adenoviral- and lentiviral-driven transcription [40], and there is now promising evidence that this approach could be successful in treating tumors. For example, Ueda et al. [41] have shown that the expression of the nitrogen-permease-like 2 (*NPRL2*) tumor-suppressor gene is restored *in vivo* in an orthotopic human lung cancer model using the US Food and Drug Administration–approved plasmid vector backbone for human clinical application, and a phase 1 clinical trial has shown the effectiveness of targeting the *FUS1* gene in stage IV lung cancer patients [42].

In conclusion, we have shown that a functional complementation approach in ovarian cancer cell lines has identified *EPB41L3* as a candidate tumor-suppressor gene for invasive ovarian cancer. We were able to demonstrate that the abrogation of *EPB41L3* in a large series of epithelial ovarian cancers was linked to promoter hypermethylation. We showed functional similarities between ovarian cancer cells in which chromosome 18 was transferred and *EPB41L3*-expressing cancer cells, suggesting that *EPB41L3* is the target on chromosome 18 that is responsible for the neoplastic suppression we observed in TOV21G cancer cells. Finally, we show that *EPB41L3* reexpression alone causes growth suppression and induces apoptotic cell death in three-dimensional models of ovarian cancer.

Acknowledgments

The authors thank Maria Notaridou for the NOSE cell line DNA, Mark Turmane for assistance with the electron microscopy, Irene Newsham for providing the Ecdysone system and the *EPB41L3* rabbit antibody. The authors also thank Ian Spendlove for use of ovarian cancer tumor tissue arrays and Claire Templeman, Michael Press, Sahar Hooshdaran, Dan Weisenberger, and Mihaela Campan for their contributions to the primary tumors methylation study.

References

[1] Stanbridge EJ and Wilkinson J (1978). Analysis of malignancy in human cells: malignant and transformed phenotypes are under separate genetic control. *Proc Natl Acad Sci USA* **75**(3), 1466–1469.

[2] Stanbridge EJ, Flandermeyer RR, Daniels DW, and Nelson-Rees WA (1981). Specific chromosome loss associated with the expression of tumorigenicity in human cell hybrids. *Somatic Cell Genet* **7**(6), 699–712.

[3] Saxon PJ, Leipzig ES, Srivatsan GV, Sameshima JH, and Stanbridge EJ (1985). Selective transfer of individual human chromosomes to recipient cells. *Mol Cell Biol* **5**(1), 140–146.

[4] Eklund LK, Islam K, Söderkvist P, and Islam MQ (2001). Regional mapping of suppressor loci for anchorage independence and tumorigenicity on human chromosome 9. *Cancer Genet Cytogenet* **130**(2), 118–126.

[5] Fukuhara H, Maruyama T, Nomura S, Oshimura M, Kitamura T, Sekiya T, and Murakami Y (2001). Functional evidence for the presence of tumor suppressor gene on chromosome 10p15 in human prostate cancers. *Oncogene* **20**(3), 314–319.

[6] Cheng Y, Chakrabarti R, Garcia-Barcelo M, Ha TJ, Srivatsan ES, Stanbridge EJ, and Lung ML (2002). Mapping of nasopharyngeal carcinoma tumor-suppressive activity to a 1.8-megabase region of chromosome band 11q13. *Genes Chromosomes Cancer* **34**(1), 97–103.

[7] Flanagan JM, Healey S, Young J, Whitehall V, Trott DA, Newbold RF, and Chenevix-Trench G (2004). Mapping of a candidate colorectal cancer tumor-suppressor gene to a 900-kilobase region on the short arm of chromosome 8. *Genes Chromosomes Cancer* **40**(3), 247–260.

[8] Gagnon A, Ripeau JS, Zvieriev V, and Chevrette M (2006). Chromosome 18 suppresses tumorigenic properties of human prostate cancer cells. *Genes Chromosomes Cancer* **45**(3), 220–230.

[9] Seitz S, Frege R, Jacobsen A, Weimer J, Arnold W, von Haefen C, Niederacher D, Schmutzler R, Arnold N, and Scherneck S (2005). A network of clinically and functionally relevant genes is involved in the reversion of the tumorigenic phenotype of MDA-MB-231 breast cancer cells after transfer of human chromosome 8. *Oncogene* **24**(5), 869–879.

[10] Ko JM, Chan PL, Yau WL, Chan HK, Chan KC, Yu ZY, Kwong FM, Miller LD, Liu ET, Yang LC, et al. (2008). Monochromosome transfer and microarray analysis identify a critical tumor-suppressive region mapping to chromosome 13q14 and THSD1 in esophageal carcinoma. *Mol Cancer Res* **6**(4), 592–603.

[11] Lung HL, Lo CC, Wong CC, Cheung AK, Cheong KF, Wong N, Kwong FM, Chan KC, Law EW, Tsao SW, et al. (2008). Characterization of a novel epigenetically-silenced, growth-suppressive gene, ADAMTS9, and its association with lymph node metastases in nasopharyngeal carcinoma. *Int J Cancer* **123**(2), 401–408.

[12] Wan M, Sun T, Vyas R, Zheng J, Granada E, and Dubeau L (1999). Suppression of tumorigenicity in human ovarian cancer cell lines is controlled by a 2 cM fragment in chromosomal region 6q24-q25. *Oncogene* **18**(8), 1545–1551.

[13] Kruzelock RP, Cuevas BD, Wiener JR, Xu FJ, Yu Y, Cabeza-Arvelaiz Y, Pershouse M, Lovell MM, Killary AM, Mills GB, et al. (2000). Functional evidence for an ovarian cancer tumor suppressor gene on chromosome 22 by microcell-mediated chromosome transfer. *Oncogene* **19**(54), 6277–6285.

[14] Cao Q, Abeysinghe H, Chow O, Xu J, Kaung H, Fong C, Keng P, Insel RA, Lee WM, Barrett JC, et al. (2001). Suppression of tumorigenicity in human ovarian carcinoma cell line SKOV-3 by microcell-mediated transfer of chromosome 11. *Cancer Genet Cytogenet* **129**(2), 131–137.

[15] Stronach EA, Sellar GC, Blenkiron C, Rabiasz GJ, Taylor KJ, Miller EP, Massie CE, Al-Nafussi A, Smyth JF, Porteous DJ, et al. (2003). Identification of clinically relevant genes on chromosome 11 in a functional model of ovarian cancer tumor suppression. *Cancer Res* **63**(24), 8648–8655.

[16] Cannistra SA (2004). Cancer of the ovary. *N Engl J Med* **351**(24), 2519–2529.

[17] Ramus SJ, Pharoah PD, Harrington P, Pye C, Werness B, Bobrow L, Ayhan A, Wells D, Fishman A, Gore M, et al. (2003). BRCA1/2 mutation status influences somatic genetic progression in inherited and sporadic epithelial ovarian cancer cases. *Cancer Res* **63**(2), 417–423.

[18] Dafou D, Ramus SJ, Choi K, Grun B, Trott DA, Newbold RF, Jacobs IJ, Jones C, and Gayther SA (2009). Chromosomes 6 and 18 induce neoplastic suppression in epithelial ovarian cancer cells. *Int J Cancer* **124**, 1037–1044.

[19] Cuthbert AP, Trott DA, Ekong RM, Jezzard S, England NL, Themis M, Todd CM, and Newbold RF (1995). Construction and characterization of a highly stable human: rodent monochromosomal hybrid panel for genetic complementation and genome mapping studies. *Cytogenet Cell Genet* **71**(1), 68–76.

[20] Li NF, Broad S, Lu YJ, Yang JS, Watson R, Hagemann T, Wilbanks G, Jacobs I, Balkwill F, Dafou D, et al. (2007). Human ovarian surface epithelial cells immortalized with hTERT maintain functional pRb and p53 expression. *Cell Prolif* **40**(5), 780–794.

[21] Neuvial P, Hupé P, Brito I, Liva S, Manié E, Brennetot C, Radvanyi F, Aurias A, and Barillot E (2006). Spatial normalization of array-CGH data. *BMC Bioinformatics* **7**, 264–266.

[22] Benjamini Y and Yekutieli D (2005). Quantitative trait loci analysis using the false discovery rate. *Genetics* **171**(2), 783–790.

[23] Høgdall EV, Christensen L, Kjaer SK, Blaakaer J, Jarle Christensen I, Gayther S, Jacobs IJ, and Høgdall CK (2008). Protein expression levels of carcinoembryonic antigen (CEA) in Danish ovarian cancer patients. *Pathology* **40**(5), 487–492.

[24] Kelm JM, Timmins NE, Brown CJ, Fussenegger M, and Nielsen LK (2003). Method for generation of homogeneous multicellular tumor spheroids applicable to a wide variety of cell types. *Biotechnol Bioeng* **83**(2), 173–180.

[25] Grun B, Benjamin E, Sinclair J, Timms JF, Jacobs IJ, Gayther SA, and Dafou D (2009). A description of a three dimensional model of ovarian and endometrial cancer. *Cell Prolif* **42**, 219–228.

[26] Lawrenson K, Benjamin E, Turmaine M, Jacobs I, Gayther S, and Dafou D (2009). *In vitro* three-dimensional modelling of human ovarian surface epithelial cells. *Cell Prolif* **42**, 385–393.

[27] Quaye L, Dafou D, Ramus SJ, Song H, Gentry-Maharaj A, Notaridou M, Hogdall E, Kjaer SK, Christensen L, Hogdall C, et al. (2009). Functional complementation studies identify candidate genes and common genetic variants associated with ovarian cancer survival. *Hum Mol Genet* **18**, 1869–1878.

[28] Coelho D, Suormala T, Stucki M, Lerner-Ellis JP, Rosenblatt DS, Newbold RF, Baumgartner MR, and Fowler B (2008). Gene identification for the *cblD* defect of vitamin B_{12} metabolism. *N Engl J Med* **358**(14), 1454–1464.

[29] Rutsch F, Gailus S, Miousse IR, Suormala T, Sagné C, Toliat MR, Nürnberg G, Wittkampf T, Buers I, Sharifi A, et al. (2009). Identification of a putative lysosomal cobalamin exporter altered in the *cblF* defect of vitamin B(12) metabolism. *Nat Genet* **41**(2), 234–239.

[30] Köbel M, Kalloger SE, Boyd N, McKinney S, Mehl E, Palmer C, Leung S, Bowen NJ, Ionescu DN, Rajput A, et al. (2008). Critical molecular abnormalities in high-grade serous carcinoma of the ovary. *Expert Rev Mol Med* **10**, e22.

[31] Kikuchi S, Yamada D, Fukami T, Masuda M, Sakurai-Yageta M, Williams YN, Maruyama T, Asamura H, Matsuno Y, Onizuka M, et al. (2005). Promoter methylation of DAL-1/4.1B predicts poor prognosis in non–small cell lung cancer. *Clin Cancer Res* **11**(8), 2954–2961.

[32] Yamada D, Kikuchi S, Williams YN, Sakurai-Yageta M, Masuda M, Maruyama T, Tomita K, Gutmann DH, Kakizoe T, Kitamura T, et al. (2006). Promoter hypermethylation of the potential tumor suppressor *DAL-1/4.1B* gene in renal clear cell carcinoma. *Int J Cancer* **118**(4), 916–923.

[33] Tsujiuchi T, Masaoka T, Sugata E, Onishi M, Fujii H, Shimizu K, and Honoki K (2007). Hypermethylation of the *Dal-1* gene in lung adenocarcinomas induced by *N*-nitrosobis(2-hydroxypropyl)amine in rats. *Mol Carcinog* **46**(10), 819–823.

[34] Schulz WA, Alexa A, Jung V, Hader C, Hoffmann MJ, Yamanaka M, Fritzsche S, Wlazlinski A, Müller M, Lengauer T, et al. (2007). Factor interaction analysis for chromosome 8 and DNA methylation alterations highlights innate immune response suppression and cytoskeletal changes in prostate cancer. *Mol Cancer* **6**, 14.

[35] Martinez-Glez V, Bello MJ, Franco-Hernandez C, De Campos JM, Isla A, Vaquero J, and Rey JA (2005). Mutational analysis of the *DAL-1/4.1B* tumour-suppressor gene locus in meningiomas. *Int J Mol Med* **16**(4), 771–774.

[36] Yi C, McCarty JH, Troutman SA, Eckman MS, Bronson RT, and Kissil JL (2005). Loss of the putative tumor suppressor band *4.1B/Dal1* gene is dispensable for normal development and does not predispose to cancer. *Mol Cell Biol* **25**(22), 10052–10059.

[37] Wong SY, Haack H, Kissil JL, Barry M, Bronson RT, Shen SS, Whittaker CA, Crowley D, and Hynes RO (2007). Protein 4.1B suppresses prostate cancer progression and metastasis. *Proc Natl Acad Sci USA* **104**(31), 12784–12789.

[38] Charboneau AL, Singh V, Yu T, and Newsham IF (2002). Suppression of growth and increased cellular attachment after expression of DAL-1 in MCF-7 breast cancer cells. *Int J Cancer* **100**(2), 181–188.

[39] Jiang W and Newsham IF (2006). Tumor suppressor DAL-1/4.1B and protein methylation cooperate in inducing apoptosis in MCF-7 breast cancer cells. *Mol Cancer* **15**, 4.

[40] Liu BH, Yang Y, Paton JF, Li F, Boulaire J, Kasparov S, and Wang S (2006). GAL4–NF-κB fusion protein augments transgene expression from neuronal promoters in the rat brain. *Mol Ther* **14**(6), 872–882.

[41] U Ueda K, Kawashima H, Ohtani S, Deng WG, Ravoori M, Bankson J, Gao B, Girard L, Minna JD, Roth JA, et al. (2006). The 3p21.3 tumor suppressor NPRL2 plays an important role in cisplatin-induced resistance in human non–small-cell lung cancer cells. *Cancer Res* **66**(19), 9682–9690.

[42] Lu C, Sepulveda CA, Ji L, Rajagopal R, O'Connor S, Jayachandran G, Hicks M, Munden R, Lee J, Templeton N, et al. (2007). Systemic therapy with tumour suppressor *FUS1*—nanoparticles for stage IV lung cancer. In: *Proceedings of the Educational Session at the 98th Annual Meeting of the American Association for Cancer Research, April 14–18, 2007. Los Angeles, CA*. American Association for Cancer Research, Philadelphia, PA. Abstract LB348.

Supplementary Information 1: References for Table 1

[1] Andersen JS, Wilkinson CJ, et al. (2003). Proteomic characterization of the human centrosome by protein correlation profiling. *Nature* **426**(6966), 570–574.

[2] Awasthi S, Singhal SS, et al. (2008). RLIP76 and cancer. *Clin Cancer Res* **14**(14), 4372–4377.

[3] Cho YL, Bae S, et al. (2005). Array comparative genomic hybridization analysis of uterine leiomyosarcoma. *Gynecol Oncol* **99**(3), 545–551.

[4] Diaz-Rodriguez E, Sotillo R, et al. (2008). Hec1 overexpression hyperactivates the mitotic checkpoint and induces tumor formation *in vivo*. *Proc Natl Acad Sci USA* **105**(43), 16719–16724.

[5] Einarson MB, Cukierman E, et al. (2004). Human enhancer of invasion-cluster, a coiled-coil protein required for passage through mitosis. *Mol Cell Biol* **24**(9), 3957–3971.

[6] Gonsalvez GB, Praveen K, et al. (2008). Sm protein methylation is dispensable for snRNP assembly in *Drosophila melanogaster*. *Rna* **14**(5), 878–887.

[7] Jiang W, Roemer ME, et al. (2005). The tumor suppressor DAL-1/4.1B modulates protein arginine *N*-methyltransferase 5 activity in a substrate-specific manner. *Biochem Biophys Res Commun* **329**(2), 522–530.

[8] Kikuchi S, Yamada D, et al. (2005). Promoter methylation of DAL-1/4.1B predicts poor prognosis in non–small cell lung cancer. *Clin Cancer Res* **11**(8), 2954–2961.

[9] Kittiniyom K, Mastronardi M, et al. (2004). Allele-specific loss of heterozygosity at the *DAL-1/4.1B* (*EPB41L3*) tumor-suppressor gene locus in the absence of mutation. *Genes Chromosomes Cancer* **40**(3), 190–203.

[10] Kolligs FT, Nieman MT, et al. (2002). ITF-2, a downstream target of the Wnt/TCF pathway, is activated in human cancers with β-catenin defects and promotes neoplastic transformation. *Cancer Cell* **1**(2), 145–155.

[11] Kuang SQ, Tong WG, et al. (2008). Genome-wide identification of aberrantly methylated promoter associated CpG islands in acute lymphocytic leukemia. *Leukemia* **22**(8), 1529–1538.

[12] Nagi C, Guttman M, et al. (2005). N-cadherin expression in breast cancer: correlation with an aggressive histologic variant-invasive micropapillary carcinoma. *Breast Cancer Res Treat* **94**(3), 225–235.

[13] Okamura K, Hagiwara-Takeuchi Y, et al. (2000). Comparative genome analysis of the mouse imprinted gene impact and its nonimprinted human homolog IMPACT: toward the structural basis for species-specific imprinting. *Genome Res* **10**(12), 1878–1889.

[14] Ota T, Suzuki Y, et al. (2004). Complete sequencing and characterization of 21,243 full-length human cDNAs. *Nat Genet* **36**(1), 40–45.

[15] Salani R, Neuberger I, et al. (2007). Expression of extracellular matrix proteins in ovarian serous tumors. *Int J Gynecol Pathol* **26**(2), 141–146.

[16] Wang SS, Smiraglia DJ, et al. (2008). Identification of novel methylation markers in cervical cancer using restriction landmark genomic scanning. *Cancer Res* **68**(7), 2489–2497.

[17] Yaqinuddin A, Abbas F, et al. (2008). Silencing of MBD1 and MeCP2 in prostate-cancer–derived PC3 cells produces differential gene expression profiles and cellular phenotypes. *Biosci Rep* **28**(6), 319–326.

[18] Yi C, McCarty JH, et al. (2005). Loss of the putative tumor suppressor band *4.1B/Dal1* gene is dispensable for normal development and does not predispose to cancer. *Mol Cell Biol* **25**(22), 10052–10059.

Supplementary Information 2: Supplementary to Figure 2*D*

Base position of CpG sites on target sequence for EPB41L3.

Amplicon 1: 0-342 bp + strand
Chromosome 18, strand start: 5533584 - strand end: 5533925, span: 342 bp
CCAGGGATCCCAGGGAGGCCCCCAGGCCGGAGGCC-GGGGCTCAGGCTCTGCGCGCCGGCCCAGCCACTACTG-CGCCGCGGCGGGCGGAGCGGGCGGGGGGCGCGGCGCG-CAGGCTCGGCCCGGTGGGGGTCCCGGCGAGCGG-GAGGGCGGTTGGGGACCCCGGCCGCGCCGGGCGCGG-GGCTCGGGATTCGGGAGACCGCGCGGCGCCGAAGC-CACGCGTCAGCCCCACTGTCCCGCGCGCCTCGCCC-CAGGCCTCGGGCTCTTCCTCCGCACCTCGTAAAGCCGA-GACCCCCTCGCAGTCCCCCACTCCGAGAGGCGGAAAAGT-TACCTGGGATCAGCAGG

Amplicon 2: 0-418 bp + strand
Chromosome 18, strand start: 5533901 - strand end: 5534318, span: 418 bp
GGAAAAGTTACCTGGGATCAGCAGGGAGCCCGGGC-GCGCCGCGGCGTGGGGACTAGGCTCGGGCGCGCGTC-CTCGGCGGCGGTGCGCAGGAGACTCGGGCGTGGGGAG-GAAGCCGCAGCCCAGGGCTGCTCGCCGCTGTTCCCCC-CGCCCCCTGTTGCAGGAGACACCGAGGCTCCGCG-GAGCTGCGGCGGGGGCCCACGCCCAGAGACCGTGCGAG-GAAAGCCAACCTCGTCCTGCCTGCCCTCCCAGCCG-CGGGGGAGGGGGCCACCGCAGTACTTCAGGACAGTTA-CATGGGCACAGCCTCCTCCGTCCTGGCGCAGGGT-CAGGCTCCGCGGACGACGCCTGGAGACAGCTGCCAATGC-CAATAGCTTTAGCCCTTTATTCCCACTTAGATGATG-GCCTGGCCTCTCCAGACCCC

Amplicon 3: 0-479 bp + strand
Chromosome 18, strand start: 5533590 - strand end: 5534068, span: 479 bp
ATCCCAGGGAGGCCCCCAGGCCGGAGGCCGGGGCT-CAGGCTCTGCGCGCCGGCCCAGCCACTACTGCGCCGC-GGCGGGCGGAGCGGGCGGGGGGGCGCGGCGCG-CAGGCTCGGCCCGGTGGGGGTCCCGGCGAGCGG-GAGGGCGGTTGGGGACCCCGGCCGCGCCGGGCGCG-GGGCTCGGGATTCGGGAGACCGCGCGGCGCCGAAGC-CACGCGTCAGCCCCACTGTCCCGCGCGCCTCGCCC-CAGGCCTCGGGCTCTTCCTCCGCACCTCGTAAAGCCGA-GACCCCCTCGCAGTCCCCCACTCCGAGAGGCGGAAAAGT-TACCTGGGATCAGCAGGGAGCCCGGGCGCGCCGCGGC-GTGGGGACTAGGCTCGGGCGCGCGTCCTCGGCGG-CGGTGCGCAGGAGACTCGGGCGTGGGGAGGAAGCCG-CAGCCCAGGGCTGCTCGCCGCTGTTCCCCCCGCCCCC-TGTTGCAGGAGACACC

Table: Genomic Locations of CpG's on the EpiTyper Target Sequence, Designed for Methylation Analysis of EPB41L3

CpG Sequenom ID*	Genomic Location (bp)
30	5533774
31	5533776
32	5533778
33	5533780
34	5533783
35	5533788
36	5533796
37	5533798
17	5534015
35	5533870
36	5533873
37	5533875
38	5533877
51	5533954
52	5533580
64	5534019
65	5534022
66	5534024

*EpiTyper assay CpG identification number, as shown in Figure 2*D*.

Table W1. *In Vitro* and *In Vivo* Phenotype Analysis of TOV21G Ovarian Cancer Cell Lines and Five TOV21G^{+18} Hybrids.

Cell Line/Hybrid	*In Vitro* Phenotype			*In Vivo* Phenotype					
				Tumor Formation (Week)[§]					Histopathologic Description of Excised Tissue[¶]
	PDs*	% CFE in Agar[†]	% Invasion[‡]	2	4	6	9	12	
TOV21G	**16.57**	6.3	0.12						Peritoneal tumor implants with ascites
21G-18.1	12.49	0	0						Adipose tissue with no signs of tumor cell infiltration
21G-18.2	12.2	0	0						Normal liver tissue with no signs of tumor cell infiltration
21G-18.3	11.31	0.49	0						Normal liver tissue and pancreatic reactive mesothelium
21G-18.4	11.64	0	0						No evidence of tumor formation
21G-18.5	11.52	0	0						Tumor implants at small intestine

*Population doublings.
[†]Colony-forming efficiency (CFE) of cells in soft agar.
[‡]The percentage of cells invading through a Matrigel. For footnotes *, †, and ‡, values represent the average obtained from three independent experiments.
[§]Abnormal tissue excised during postmortem analysis of one animal killed at each time point, then analyzed by a histopathologist. Dark gray boxes indicate excised tissue was infiltrated by tumor cells; light gray boxes indicate excised tissue was nonneoplastic; white boxes indicate no evidence of abnormal tissue.
[¶]Histopathlogical description of excised tissue.

Table W2. Table Showing Percent of Total Tumor Samples Analyzed across Three Tumor Tissue Collections (Danish MALOVA Study, Derby City Hospital Tumor Array, and Newcastle Ovarian Cancer Tissue Microarray) with Their Corresponding Levels of Staining for EPB41L3 Antibody.

Histologic Subtype	Levels of EPB41L3 Staining*			
	0	1	2	3
Serous (n = 454)	66.3	19.6	9.3	4.8
Mucinous (n = 70)	61.4	17.2	14.2	7.1
Endometrioid (n = 150)	56.6	22	11.4	10
Clear cell (n = 61)	68.9	16.4	9.8	4.9
Undifferentiated (n = 38)	26.3	49.9	15.7	7.9
Papillary (n = 21)	38.0	28.5	23.8	0.4
Benign (n = 33)	24	16	6	54

*Staining values: 0, less than 5% of neoplastic cells stain positive; 1, 5% to 20%; 2, 20% to 50%; 3, more than 50%.

Supplementary Information 3: Verifying the Phenotypic Effects of Overexpression of EPB41L3 in Ovarian Cancer Cell Lines

(Figures W1 to Figures W3)

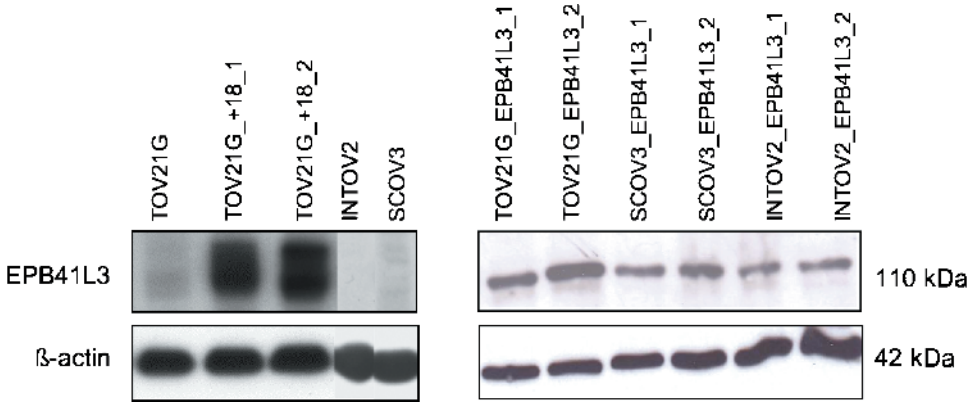

Figure W1. Confirming the expression of EPB41L3 after transfection into ovarian cancer cell lines TOV21G, INTOV2, and SCOV3. All three cell lines show little or no EPB41L3 expression compared with two clones generated for each cell line expressing the EPB41L3 full-length cDNA. Data are also shown for the two MMCT-18 hybrids generated from TOV21G, which express EPB41L3.

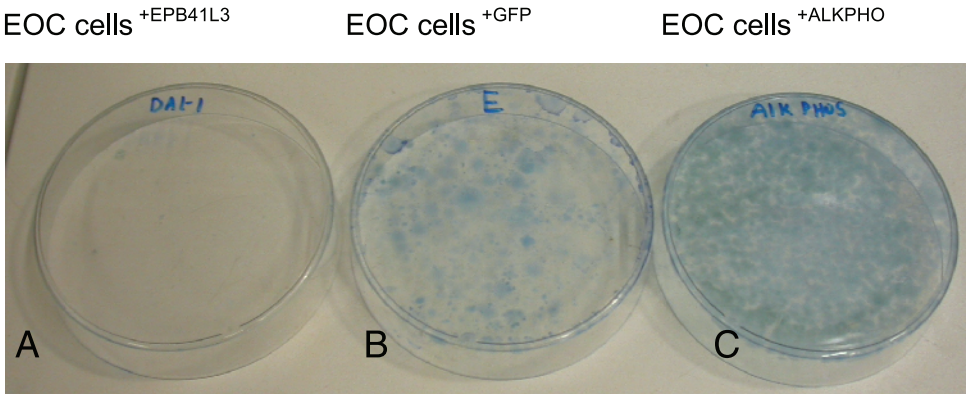

Figure W2. Anchorage-dependent colony formation assays of an epithelial ovarian cancer (EOC) cell line (TOV21G) transfected with a plasmid expressing EPB41L3 (A), a GFP-labeled empty vector (control 2; B), and an alkaline phosphatase–expressing vector (control 2; C). There are clear differences in the ability of EPB41L3-expressing EOC cells to form colonies compared with both controls as shown by the extent of bromophenol blue–stained colonies formed after EPB41L3 transfection. There is hardly any evidence of viable cell growth and colony formation in EPB41L3-expressing cells.

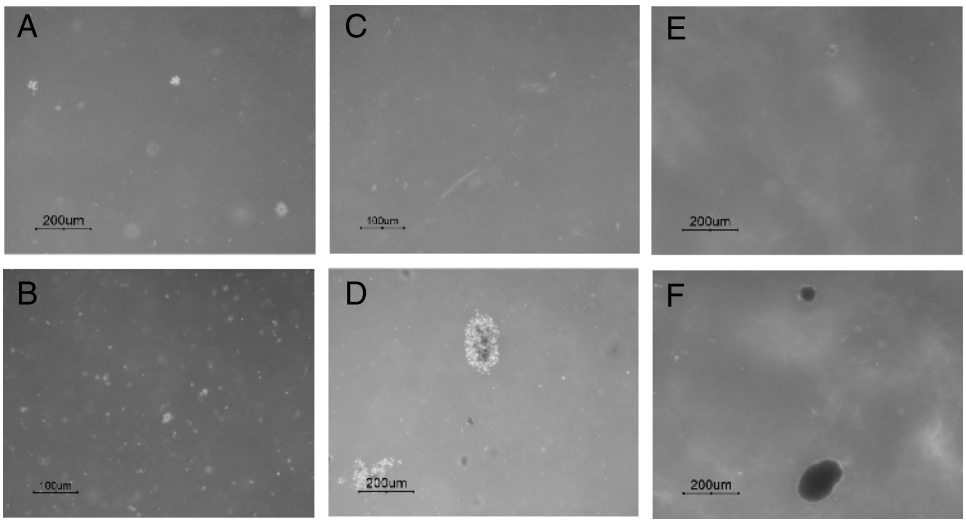

Figure W3. Anchorage-independent colony formation after overexpression of EPB41L3 in three EOC cell lines. In all three instances, expression of EPB41L3 in two-dimensional EOC cell line led to a suppression of their ability to form colonies in soft agar: (A) TOV21G$^{+EPB41L3}$, (B) TOV21G, (C) INTOV2$^{+EPB41L3}$, (D) INTOV2, (E) SCOV3$^{+EPB41L3}$, and (F) SCOV3.